Imaging Consecutive Steps of O_2 Reaction with Hydroxylated $TiO_2(110)$: Identification of HO_2 and Terminal OH Intermediates

Yingge Du,[†] N. Aaron Deskins,[‡] Zhenrong Zhang,[‡] Zdenek Dohnálek,[‡] Michel Dupuis, and Igor Lyubinetsky*,[†]

Environmental Molecular Sciences Laboratory, Fundamental and Computational Sciences Directorate, Institute for Interfacial Catalysis, and Pacific Northwest National Laboratory, Richland, Washington 99352

Received: August 6, 2008; Revised Manuscript Received: September 5, 2008

We report the results of a combined experimental and theoretical investigation of the reaction of molecular oxygen with a partially hydroxylated $TiO_2(110)$ surface. The consecutive steps of both primary and secondary site-specific reactions have been tracked with high-resolution scanning tunneling microscopy (STM). We have directly imaged stable, adsorbed hydroperoxyl (HO_2) species, which is believed to be a key intermediate in many heterogeneous photochemical processes but generally metastable and "elusive" until now. We also found terminal hydroxyl groups, which are another critical but never previously directly observed intermediates. Conclusive evidence that O_2 reacts spontaneously with a single bridging OH group as an initial reaction step is provided. The experimental results are supported by density functional theory (DFT) calculations that have determined the energies and configurations of these species. Reported observations provide a base for a consistent description of the elementary reaction steps and offer molecular-level insight into the underlying reaction mechanisms. Tthe results are also expected to have important implications for various catalytic systems involving the interconversion of O_2 and H_2O.

Introduction

Oxygen and water are two of the most prevalent and important chemicals on our planet. As such, their chemical interactions have attracted great interest from both fundamental and technological points of view. Although the production of H_2 and O_2 via photocatalytic water splitting holds promise in providing renewable, clean energy,[1] in a broader perspective, the reduction of O_2 to H_2O plays a vital role in many important chemical and biological processes, ranging from combustion[2] and atmospheric reactions,[3] to oxygen radical biology[4] and degradation of organic pollutants.[5] Reactions leading from O_2 to H_2O or vice versa (in particular, on catalytically active surfaces) often involve intricate mechanisms with a number of possible surface-bound reactive intermediates, such as OH, HO_2, or H_2O_2.[4,6,7] In general, such reactions on surfaces are challenging to explore with ensemble-averaging spectroscopic techniques because of the relatively small number of participating molecules and the difficulty in resolving intermediates spectroscopically.

In numerous studies of heterogeneous photocatalytic water splitting, titania (TiO_2) has emerged as an important model system because of its superior photocatalytic properties and as a prototypical metal oxide. It is recognized that both TiO_2 photocatalytic activity and O_2 effectiveness as a scavenger of photoexited electrons are affected by the presence of surface hydroxyl groups.[8,9] (Molecular oxygen is generally recognized as an effective scavenger of photoexited electrons that prevents photocatalyst deactivation by negative charge accumulation.) Recently, a number of studies have focused on fundamental aspects of the interaction of oxygen and water on the reduced rutile $TiO_2(110)$ surface[10–15] that can be easily hydroxylated via

water dissociation at oxygen vacancies. Several studies have speculated or invoked the existence of Ti-bonded metastable HO_2/H_2O_2 and terminal OH species as intermediates in these processes.[10–13] However, direct evidence for these species and reactions leading to their formation has not been available to date.

As a key step in this direction, we followed the consecutive reactive steps of O_2 with a partially hydroxylated $TiO_2(110)$ surface via high-resolution scanning tunneling microscopy (STM). We report here the first direct imaging of two key O-containing species adsorbed at terminal Ti sites and identify them as hydroperoxyls, HO_2, and terminal hydroxyls, OH_t. By tracking species that result from a sequence of primary and secondary reactions and comparing results with density functional theory (DFT) calculations, we extract molecular-level details about the underlying reaction mechanism.

Experimental Section

Experiments in this study were performed in two separate ultrahigh vacuum (UHV) STM systems[16,17] which have similar setups; thus, only one is described in a detail here. System I (base pressure 3×10^{-11} Torr) is equipped with a variable-temperature STM (Omicron), a semispherical electron energy analyzer (Omicron), a mass spectrometer (Ametek), and electron and ion guns (VG and SPECS, respectively).[16] The single-crystal rutile $TiO_2(110)$-(1×1) surface (Princeton Scientific) was prepared by multiple cycles of Ar ion sputtering (2 keV) and UHV annealing (800–900 K), with cleanliness monitored by X-ray photoelectron and Auger electron spectroscopies. At the beginning of each experiment, the sample was flash-annealed to 600 K. Partially hydroxylated $TiO_2(110)$ surfaces were obtained by either H_2O dosing through a dedicated doser or waiting for water dissociation from UHV background (in both cases, the obtained results have correlated with each other). The

---

* Corresponding author. E-mail: igor.lyubinetsky@pnl.gov.
[†] Environmental Molecular Sciences Laboratory.
[‡] Fundamental and Computational Sciences Directorate.

dosed water was degassed by freeze−pump−thaw cycles prior to use. The interaction of O$_2$(g) with the hydroxylated TiO$_2$(110) surface was studied at 300 K. Oxygen was introduced using a movable directional doser connected to a 1-mm-i.d. tube that terminated 3 mm from the STM tunneling junction. Because of a tip shadow effect, we have not used an absolute (calibrated) oxygen flux, but rather, a dosing time as a measure of O$_2$ exposure. The vacancy concentration and species coverage were obtained by a direct counting from STM images and expressed in monolayer (ML) units (1 ML corresponds to 5.2×10^{14} cm^{-2} Ti atoms). STM tips were homemade from electrochemically etched W wire and cleaned in situ by annealing and ion sputtering. Presented STM (empty state) images were collected in a constant-current (0.1−0.3 nA) mode at positive sample bias voltages of 1.5−1.8 V. The resulting images were processed using WSxM software.[18]

Computational Details

We performed density functional theory calculations using the Vienna ab initio software package (VASP)[19] in conjunction with the PBE functional.[20] Core electrons were represented by projector augmented-wave potentials,[21] whereas valence electrons were described by a plane-wave basis set with a cutoff energy of 400 eV. We used a slab model with four O−Ti−O layers and a (2 × 3) surface supercell to describe the surface. The dimensions of this cell were 13.16 Å × 8.91 Å × 30 Å, giving a vacuum gap of ∼18 Å for the clean surface. The top two layers of the slab were allowed to relax. The Brillouin zone was sampled by a single k-point. Tests with a 2 × 2 × 1 k-point mesh gave results equivalent to those using a 1 × 1 × 1 k-point mesh.

The STM line profiles were generated using the Tersoff−Hamann approximation.[22] The method assumes that the tunneling current is proportional to the density of states within the range of the energy scan. A problem inherent in periodic DFT calculations, due to numerical artifacts, is that the zero of energy for the Kohn−Sham eigenvalues is not the same for different systems, so the band structures need to be shifted to the same scale. Because the adsorbate concentration is not in the dilute limit, the Fermi level can also unreasonably shift due to the presence of the adsorbate. To overcome these difficulties, we aligned the band structures relative to a clean surface and used the clean surface Fermi level as the Fermi level for the adsorbate/surface systems. We generated densities from the Fermi level up to a positive bias of 1.8 eV above the Fermi level. The STM line profiles were plotted for a density of 6×10^{-6} e/Å^3. Importantly, different energy ranges and density contours showed the same trends in the peak heights of the line profiles.

Results and Discussion

A typical STM image of the partially hydroxylated TiO$_2$(110) surface (OH coverage, ∼0.04 ML) before O$_2$ exposure is shown in the inset of Figure 1a. The image of TiO$_2$(110) is dominated by electronic contrast where the low lying rows of terminal, 5-fold coordinated Ti atoms appear bright, counter to intuition, and high lying bridging oxygen (O$_b$) rows appear dark.[23] Beyond the periodic surface structure, brighter bridging hydroxyls (OH$_b$) and less bright bridging oxygen vacancies (O$_{vac}$) can be recognized on the dark O$_b$ rows (marked with squares), in accord with previous reports in the literature.[24,25] The O$_{vac}$'s (here, ∼0.09 ML) are a result of the partial reduction of TiO$_2$ during sample preparation with ion sputtering and vacuum annealing. In turn, the OH$_b$'s result from H$_2$O dissociation at O$_{vac}$'s,

$$H_2O + O_{vac} + O_b \rightarrow 2OH_b$$
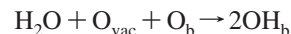
and as the reaction scheme suggests, OH$_b$'s appear in pairs upon their creation, as shown in Figure 1a (as one large spot labeled 2OH$_b$).[24,25] There are two known mechanisms leading to the separation of the OH$_b$ pairs to isolated OH$_b$ groups: cross-row hydrogen diffusion assisted by molecularly bound H$_2$O[26] and intrinsic along-row hydrogen diffusion.[17]

To investigate the surface reactions between OH$_b$'s and O$_2$(g), we exposed the partially hydroxylated surface (0.04 ML of OH$_b$'s) to O$_2$ at 300 K, and the resulting STM image is displayed in Figure 1a. Three new features (marked with circles) can be seen on the Ti rows. The small bright spots (dotted circles) are assigned to O adatoms (O$_a$), which are known to be a direct result of O$_2$ dissociation on O$_{vac}$ sites.[14,16,27,28] (One oxygen atom of O$_2$ fills the vacancy, and the other atom resides as an O$_a$ on Ti row.) In this report, we will provide evidence that O adatoms on Ti rows can form also as a result of reactions of molecular oxygen with bridging hydroxyl groups.

The other two features result from reactions of partially hydroxylated TiO$_2$(110) with O$_2$(g). They are HO$_2$ (dashed circles, Figure 1a) and OH$_t$ (solid circles). The detailed explanation of our assignment is provided below along with the discussion of Figures 2−6. Here, we focus on the relative appearance and position of all of the features (O$_{vac}$, OH$_b$, O$_a$, HO$_2$, and OH$_t$) observed in the STM images. The cross-row line profiles are provided in Figure 1b to quantitatively illustrate the observed differences. The empty-state, bias-dependent appearances of OH$_b$'s and O$_{vac}$'s, which are both centered on
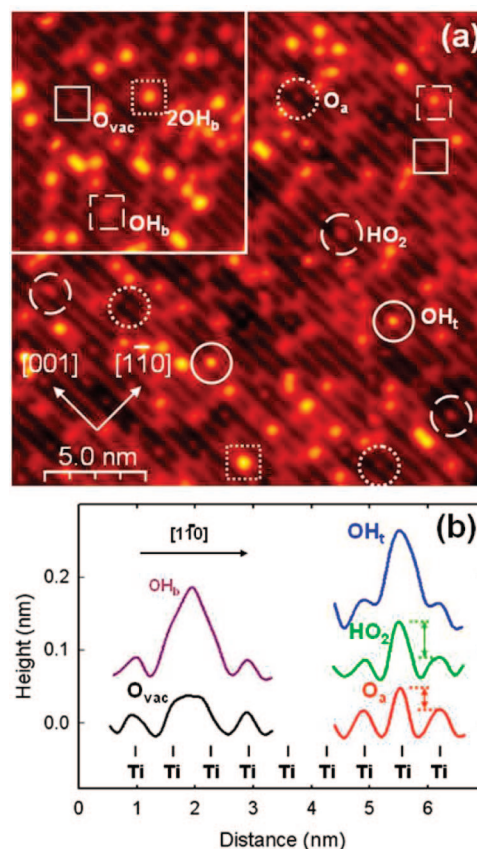
Figure 1. (a) STM empty-state image of partially hydroxylated (0.04 ML) TiO$_2$(110) surface after 14 min of exposure to O$_2$. Inset shows a partially hydroxylated surface before O$_2$ exposure. (b) Averaged line profiles along the [1-10] direction of the different surface features. (Profiles are vertically displaced for ease of viewing, and the measurement of feature height is illustrated).
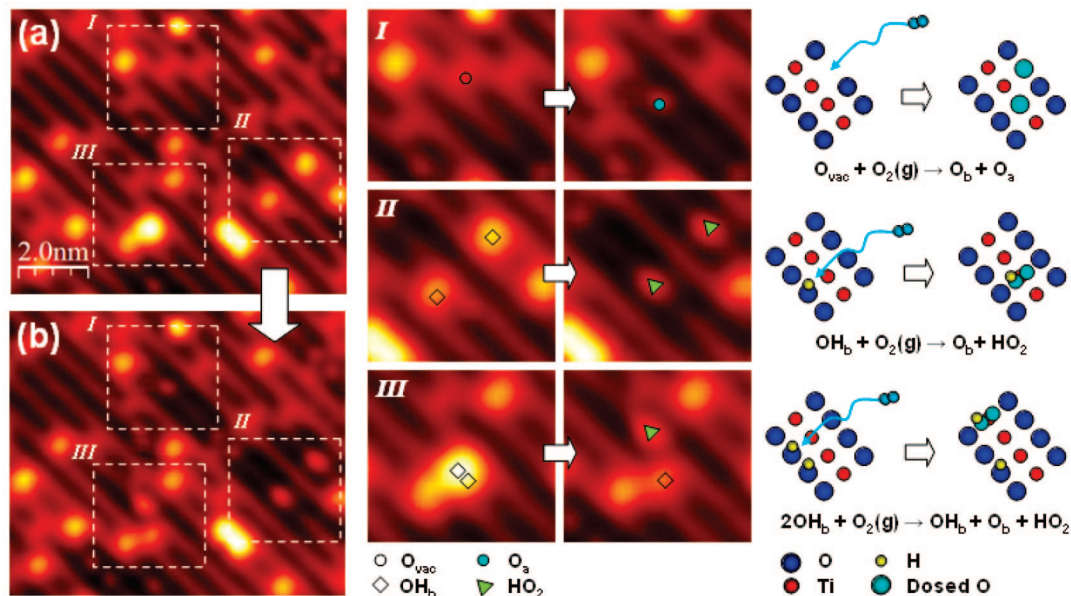
Figure 2. (a, b) Two STM images of the same area after O$_2$ exposure for 9 and 14 min, respectively. Magnified images of three different areas (I, II, III) from panels a and b and atomistic ball models are presented to illustrate the surface reactions.

O$_b$ rows, have been extensively studied.[24,25,29] Generally, at a typical tunneling bias (1−2 V), the OH$_b$ feature is higher than O$_{vac}$, as shown in the line scans plotted in the left part of Figure 1b. The line profiles for the Ti-centered features are shown in the right part of Figure 1b; the feature height, measured relative to the top of the neighboring Ti row, is the largest for OH$_t$ (0.09 ± 0.2 nm), followed by the HO$_2$ (0.05 ± 0.1 nm) and the O$_a$ (0.03 ± 0.1 nm). Spatially, both O$_a$ and OH$_t$ appear round, but HO$_2$ is slightly elongated along the Ti row.

In what follows, we focus on the assignments of the O$_a$, HO$_2$, and OH$_t$ features on the basis of the changes observed on the same area of the surface before and after step-by-step O$_2$ doses. Knowledge of the original positions of the O$_{vac}$'s and OH$_b$'s is proving critical in resolving the assignments and in tracking site-specific reactions. Figure 2a and b displays two images of the identical surface area after 9 and 14 min O$_2$ doses, respectively. Magnified views of three specific areas (labeled I, II, and III), marked to point out the features that have changed, are shown in the middle of Figure 2. Additionally, ball models are displayed alongside to illustrate the surface reactions assigned to these changes.

Changes in area I, Figure 2, illustrate the O$_a$ formation via O$_2$ dissociation on O$_{vac}$ sites:[14,16,27]

$$O_{vac} + O_2(g) \rightarrow O_b + O_a \tag{1}$$
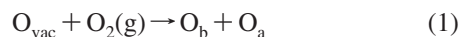
Here, the original O$_{vac}$ is healed by one oxygen atom of an O$_2$ molecule, with the other atom deposited on the neighboring Ti row as an adatom, O$_a$. Note that the O$_a$ is shifted by one lattice constant from the original O$_{vac}$ along the [001] direction (see the corresponding ball models). We have shown previously[16] that this is the most probable O$_a$ configuration (relative to O$_{vac}$), resulting from a transient mobility of the hyperthermal O$_a$ upon O$_2$ dissociation at O$_{vac}$ sites.

Changes in area II, Figure 2, show two events involving reactions of isolated OH$_b$ with O$_2$(g), whereby the OH$_b$ group is converted to O$_b$ and a new feature appears on the adjacent Ti row. A similar reaction takes place in area III. There, a pair of OH$_b$ species is initially present, and then a H atom from one OH$_b$ group disappears. The same new feature as observed in area II is detected on a nearby Ti site, while a single OH$_b$ is
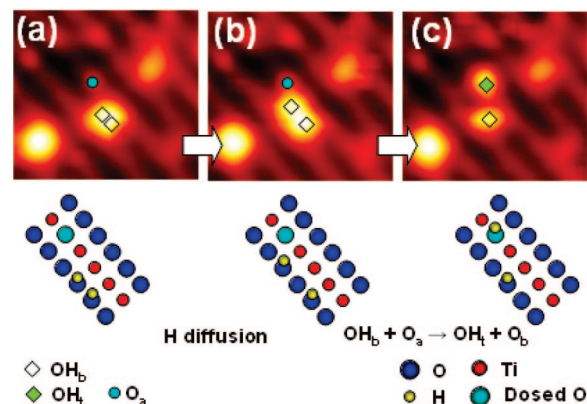
Figure 3. Time-lapse STM images of (3.5 × 3.2) nm^2 area scanned after stopping O$_2$ dosing with time stamps of (a) 0, (b) 4, and (c) 8 min, illustrating the formation of OH$_t$ through H diffusion along the O$_b$ row and transfer to the adjacent O$_a$ (reaction 3).

still seen to be located on the O$_b$ row. These changes indicate that a H atom of the OH$_b$ group has reacted with the O$_2$(g) in both areas II and III. A reaction that is consistent with the overall stoichiometry can be written as

$$OH_b + O_2(g) \rightarrow O_b + HO_2 \tag{2}$$

suggesting that the new species might be HO$_2$, hydroperoxyl. (Further observations discussed below will confirm this assignment.) A key finding from our results is that HO$_2$ is formed by reaction of O$_2$(g) with both an isolated OH$_b$ (see area II of Figure 2) and paired OH$_b$'s (area III of Figure 2). Earlier DFT work had suggested that only reactions of O$_2$ with a pair of OH$_b$'s should lead to a stable HO$_2$ (and H$_2$O$_2$) species.[12] Our observations provide evidence that in an initial reaction step, O$_2$ reacts directly and spontaneously with a single bridging OH group to form HO$_2$.

The formation of the second new feature, terminal Ti-bound hydroxyl OH$_t$, is revealed in Figure 3, which displays a sequence of three STM images taken after stopping the O$_2$ dosing. The first image, Figure 3a, shows a pair of OH$_b$'s and a single O$_a$ formed by the preceding O$_2$ exposure. In the second image, Figure 3b, the H atom from the top OH$_b$ has moved one lattice
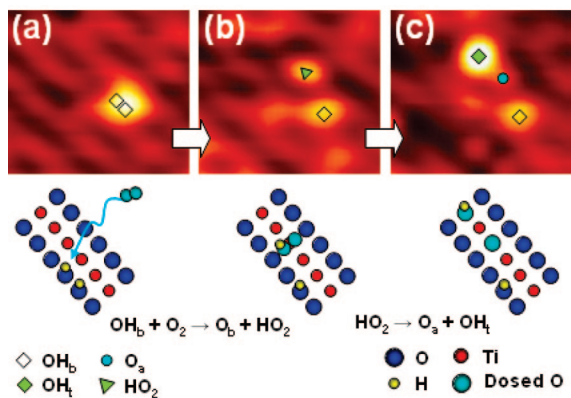
Figure 4. Time-lapse STM images of (4.3 × 2.7) nm^2 area imaged during O$_2$ dosing with time stamps of (a) 0, (b) 12, and (c) 64 min, illustrating reaction 4. Following HO$_2$ formation (a to b), after awhile, the HO$_2$ spontaneously dissociates (b to c) to form O$_a$ and OH$_t$ species.

Figure 5. Time-lapse STM images of (2.9 × 2.8) nm^2 area after O$_2$ dosing of (a) 9 and (b) 14 min, illustrating reaction 5. Two OH$_b$ groups in panel a are replaced in panel b by an O$_a$ and two adjacent OH$_b$ groups resulting from H$_2$O dissociation at nearby O$_{vac}$. The model in the dashed box schematically shows an assumed but not captured initial event of HO$_2$ formation via reaction 2.

constant up along the O$_b$ row, which brings it in close proximity to the O$_a$ species. (Intrinsic H diffusion along OH$_b$ rows has been investigated in our recent study.[17]) When OH$_b$ location is in the vicinity of the O$_a$, both species participate in further reactions: the H atom from the OH$_b$ group disappears, and a new bright feature appears at the position of O$_a$, which we assign to OH$_t$ in Figure 3c. Since the latter process occurs *without O$_2$ flowing*, the observed change has to be due to an H transfer from OH$_b$ to O$_a$, creating OH$_t$ as a result.

$$O_a + OH_b \rightarrow OH_t + O_b \qquad (3)$$

Although the existence of OH$_t$ has been proposed in a number of previous studies,[11,30,31] this is the first direct observation of this species by STM. In a side comment to reaction 3, illustrated in Figure 3b and c, note that we cannot exclude the possibility that H diffuses one more lattice constant up and then H transfer happens spontaneously, since we have never observed OH$_b$ and O$_a$ at nearest adjacent sites. (A similar observation is valid for a secondary reaction 5, described later.) Note also that observing OH$_t$ formation *during O$_2$ dosing* revealed a small increase in the number of detected events in comparison with the case without O$_2$ flowing. We attribute this to a possible minor reaction channel involving an intermediate HO$_2$ formation adjacent to O$_a$ site (via reaction 2), reacting to form OH$_t$ according to modified reaction 3.

$$O_a + OH_b + O_2(g) \rightarrow O_a + HO_2 + O_b \rightarrow OH_t + O_2(g) + O_b$$

Both new Ti-bonded HO$_2$ and OH$_t$ species are observed to be quite stable and immobile at 300 K and can be imaged over extended periods of time (>60 min). However, in a few instances, we observed HO$_2$ dissociation into O$_a$ and OH$_t$ according to

$$HO_2 \rightarrow O_a + OH_t \qquad (4)$$

The STM image sequence illustrating this reaction is shown in Figure 4, where panels a and b display the initial event of HO$_2$ formation at this site (via reaction 2). HO$_2$ spontaneous dissociation can be seen in panels b and c. Reaction 4 provides strong additional evidence for the chemical makeup of the HO$_2$ species. We believe that the first direct observation of HO$_2$ species also validates the interpretation of the pioneering TPD studies by Henderson, in which HO$_2$ had been postulated to be an intermediate in the reactions of O$_2$ with OH$_b$ groups on TiO$_2$(110).[10,11]

Reaction 2 is the primary process that leads to the formation of HO$_2$ species when hydroxylated TiO$_2$(110) is exposed to O$_2$(g). However, when another OH$_b$ is present in the vicinity of HO$_2$, our observations indicate that a secondary reaction may occur, with the formation of O$_a$ and H$_2$O.

$$OH_b + HO_2 \rightarrow O_b + O_a + H_2O \qquad (5)$$
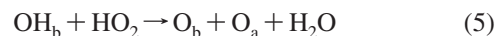
Since molecularly bound H$_2$O is very mobile at 300 K,[24,25] it can not be imaged with STM. The evidence for H$_2$O formation comes from its immediate dissociation on a nearby O$_{vac}$ site. The overall sequence of events can thus be written as follows:

$$OH_b + HO_2 \rightarrow O_b + O_a + H_2O \qquad H_2O + O_{vac} +$$
$$O_b \rightarrow 2OH_b$$
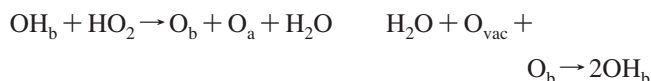
In about 85% of cases, we have, indeed, observed the dissociation of a newly created H$_2$O molecule on a neighboring O$_{vac}$. We consider this to be strong confirmation that the identified H$_2$O molecules are direct products of reaction 5 and do not originate from the UHV background. The initial reactants and final products for reaction 5 are shown in the STM images in Figure 5. Although the initial event of HO$_2$ formation via reaction 3 is not imaged here by *scanning after O$_2$ exposure* (because of the related time delay), we have been able to detect it by *scanning during O$_2$ dosing* (albeit with lower resolution), as shown in Figure S1 of the Supporting Infomation, confirming the reaction mechanism. Note also that the above results indicate that, on partially hydroxylated reduced TiO$_2$(110), O$_a$'s could be formed not only via O$_2$ dissociation at O$_{vac}$ sites (reaction 1), but also as a result of HO$_2$ dissociation (reaction 4) and HO$_2$ reacting with nearby OH$_b$ (reaction 5).

A side note to reaction 5 is that from our experiments, it is unclear whether the short-lived hydrogen peroxide (H$_2$O$_2$) intermediate is present before O$_a$ and H$_2$O formation, as discussed in the literature.[30,32,33] The fact that we do not observe H$_2$O$_2$ as an intermediate in this reaction suggests that if it exists, its lifetime is short as compared to our STM sampling rate (2 min/frame). The short lifetime is in accord with the results of electron paramagnetic resonance studies that show that H$_2$O$_2$ decomposes when in contact with TiO$_2$.[34]

Similar to the secondary reaction 5 between HO$_2$ and OH$_b$, the OH$_t$ and OH$_b$ species can also recombine when the OH$_b$
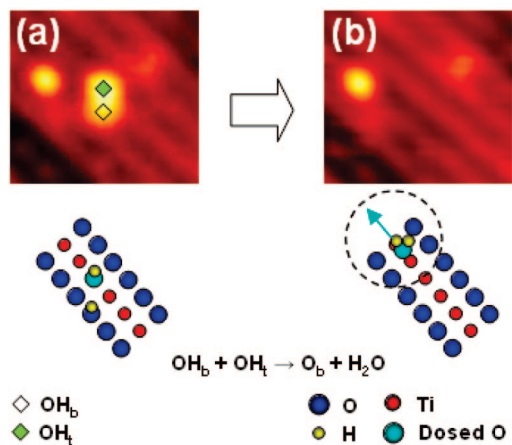
Figure 6. Consecutive time-lapse STM images of (3.5×3.2) nm^2 area recorded after O$_2$ dosing (time between images is 2 min). The neighboring OH$_b$ and OH$_t$ species in panel a have disappeared in panel b, illustrating reaction 6. The dashed circle in the model schematically shows an assumed but not captured here event of HO$_2$ formation and subsequent diffusion.

location is in the vicinity of the OH$_t$, and we have, indeed, observed this reaction with the formation of H$_2$O.

$$OH_b + OH_t \rightarrow O_b + H_2O \qquad (6)$$
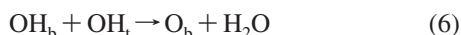
(In the same way, mobile molecularly bound H$_2$O may be detected from its dissociation on a nearby O$_{vac}$ site). Reaction 6 is illustrated in Figure 6, which displays that both initial species of OH$_t$ and OH$_b$ in panel a undergo further reactions: the H atom from the OH$_b$ group and the entire OH$_t$ feature disappear in panel b.

Although, as mentioned above, the OH$_t$ species is immobile and stable at 300 K, it is possible that two adjacent OH$_t$ groups can further recombine (if their concentrations are sufficient or if the temperature is increased),

$$OH_t + OH_t \rightarrow H_2O + O_a$$
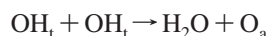
also producing water as a final product.[11] Indirect experimental evidence in the literature strongly supports such a mechanism.[11,30] In particular, this reaction, together with water producing reactions 5 and 6, would be consistent with previous TPD studies, in which a new H$_2$O desorption feature at >300 K has been observed.[10,11] We currently do not have direct evidence for such a OH$_t$ recombination process, most likely because of a low initial OH$_b$ coverage or slow species diffusion. Further STM studies on fully hydroxylated surfaces, or at elevated temperatures (or both) are thus warranted. However, described above are five primary and secondary elementary reaction steps (reactions 2−6), which for the first time have been visualized at the atomic level, provide a basis for consistent description of the O$_2$ interaction with hydroxylated TiO$_2$(110) surface.

To further support our assignments, we performed DFT calculations of Ti-bonded HO$_2$ and OH$_t$ surface species. Our calculations show that both HO$_2$ and OH$_t$ can exist as stable species adsorbed on the surface, as shown in Figure 7. Reaction 2 of an O$_2$ molecule with a single OH$_b$ species to form a Ti-bonded HO$_2$ moiety is predicted to be exothermic by −0.66 eV. This stable conformation of the HO$_2$ species adsorbed directly on top of a 5-fold coordinated Ti atom has a monodentate Ti−O bond and a strong hydrogen bond to a nearby O$_b$ atom ("transverse" conformation) (Figure 7a). Our structure is markedly different from a previously reported unstable structure of HO$_2$ that was much flatter over the surface.[12] We also
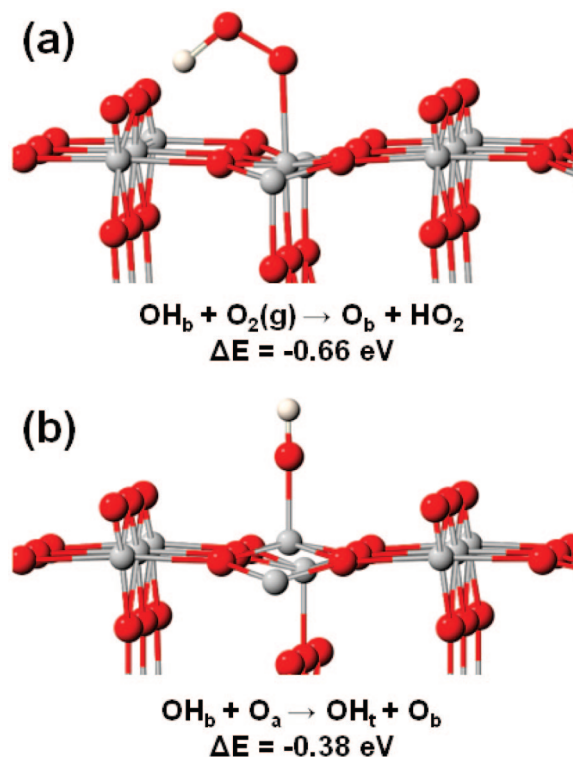
Figure 7. Optimized structures of species on the rutile TiO$_2$(110) surface: (a) HO$_2$ and (b) OH$_t$. Corresponding reactions and their energies are shown underneath. Red spheres represent O atoms; white spheres, H atoms; and gray spheres, Ti atoms.
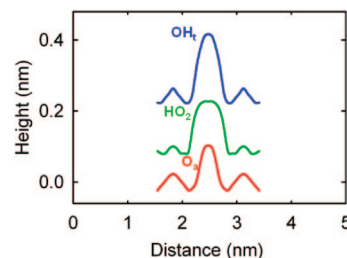
Figure 8. Simulated STM line profiles at +1.8 V bias along the [1-10] direction for all Ti-bonded species of HO$_2$, OH$_t$, and O$_a$.

explored such a structure with calculations and found it energetically unfavorable (with formation energy of 0.08 eV). Consistent with the earlier work[12] as well, the presence of a second OH$_b$ species near the adsorbed HO$_2$ was found to lead to an increased stability of $\sim$1.0 eV for the reaction

$$2OH_b + O_2(g) \rightarrow OH_b + O_b + HO_2$$
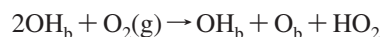
(Experimental evidence for this process was discussed earlier; see area III in Figure 2.) Note that the transverse structure does not agree completely with STM appearance of the HO$_2$ feature (elongated along Ti row). Although we have also found an HO$_2$ stable structure aligned along the Ti row, it is less thermodynamically favorable (ΔE of −0.09 eV) (Figure S2 of the Supporting Information). Nevertheless, our calculations indicate that an isolated HO$_2$ species can exist on the surface. The optimized structure for the second new species, a terminal hydroxyl group, is shown in Figure 7b. Reaction 4 for formation of OH$_t$ by H transfer from OH$_b$ to O$_a$ is calculated to be exothermic by $\sim$0.38 eV.

To compare the experimentally observed appearance of HO$_2$, OH$_t$, and O$_a$ species with the theory, we employed the Tersoff−Hamann approach[22] and calculated isodensity contours

O₂ Reaction with Hydroxylated TiO₂(110)

J. Phys. Chem. C, Vol. 113, No. 2, 2009 **671**

resulting from the empty states in an energy range between the Fermi level and +1.8 eV, as shown in Figure 8. The projected densities of states for these species (used to create the STM line profiles) are displayed in Figure S3 of the Supporting Information. Simulated STM line profiles show that the OH_t feature is the highest, followed by HO_2 and then O_a, in qualitative agreement with the experimental profiles in Figure 1b (further details for the HO_2 STM profile calculations are given in the Supporting Information).

Summary

We have performed a combined experimental and theoretical investigation of the reaction of molecular oxygen with a partially hydroxylated TiO₂(110) surface. Using high-resolution STM imaging, we have directly monitored the initial surface defects (oxygen vacancies and bridging hydroxyls) and tracked (atom-by-atom) changes caused by the interaction of single O₂ molecules. Both primary and secondary reactions (five overall) have been visualized at an atomic level, and the identification of two key reactive intermediates of HO_2 and OH_t provides a basis for the self-consistent description of the elementary reaction steps. We provide conclusive evidence that O₂ reacts spontaneously with a single bridging OH group as an initial reaction step. The experimental results are complemented by density functional theory calculations that have determined the energies and configurations of these species and support our assignments. We believe that the direct observation of adsorbed HO_2 and OH_t species reported here opens an important research avenue for characterization of molecular-level details of catalytic interconversions of O₂ and H₂O. In a broader perspective, we envision that our observations and findings have implications with regard to many heterogeneous catalytical processes and applications, including hydrogen production via water splitting.

Supporting Information Available: Complementary STM image illustrating reaction 5, further computational details, calculated geometries, and bond distances for various HO_2 structures and projected densities of states. This information is available free of charge via the Internet at http://pubs.acs.org.

References and Notes

(1) Fujishima, A.; Honda, K. *Nature* **1972**, *238*, 37.
(2) Mueller, M. A.; Kim, T. J.; Yetter, R. A.; Dryer, F. L. *Int. J. Chem. Kinet.* **1999**, *31*, 113.
(3) Zuo, Y.; Hoigne, J. *Environ. Sci. Technol.* **1992**, *26*, 1014.
(4) Fridovich, I. *Science* **1978**, *201*, 875.
(5) Bielanski, A.; Haber, J. *Oxygen in Catalysis*; Dekker: New York, 1991.
(6) Henderson, M. A. *Surf. Sci. Rep.* **2002**, *46*, 1.
(7) Sivadinarayana, C.; Choudhary, T. V.; Ldaemen, L.; Eckert, J.; Goodman, D. W. *J. Am. Chem. Soc.* **2004**, *126*, 38.
(8) Linsebigler, A. L.; Lu, G. Q.; Yates, J. T., Jr. *Chem. Rev.* **1995**, *95*, 735.
(9) Fu, X.; Zeltner, W. A.; Anderson, M. A. *Stud. Surf. Sci. Catal.* **1996**, *103*, 445.
(10) Epling, W. S.; Peden, C. H. F.; Henderson, M. A.; Diebold, U. *Surf. Sci.* **1998**, *412/413*, 333.
(11) Henderson, M. A.; Epling, W. S.; Peden, C. H. F.; Perkins, C. L. *J. Phys. Chem. B* **2003**, *107*, 534.
(12) Tilocca, A.; DiValentin, C.; Selloni, A. *J. Phys. Chem. B* **2005**, *109*, 20963.
(13) Zhang, C.; Lindan, P. J. D. *J. Chem. Phys.* **2004**, *121*, 3811.
(14) Wendt, S.; Schaub, R.; Matthiesen, J.; Vestergaard, E. K.; Wahlstrom, E.; Rasmussen, M. D.; Thostrup, P.; Molina, L. M.; Lagsgaard, E.; Stensgaard, I.; Hammer, B.; Besenbacher, F. *Surf. Sci.* **2005**, *598*, 226.
(15) Qu, Z.; Kroes, G. J. *J. Phys. Chem. B* **2006**, *110*, 23306.
(16) Du, Y.; Dohnalek, Z.; Lyubinetsky, I. *J. Phys. Chem. C* **2008**, *112*, 2649.
(17) Zhang, Z.; Bondarchuk, O.; Kay, B. D.; White, J. M.; Dohnalek, Z. *J. Phys. Chem. B* **2006**, *110*, 21840.
(18) Horcas, I.; Fernandez, R.; Gomez-Rodriguez, J. M.; Colchero, J.; Gomez-Herrero, J.; Baro, A. M. *Rev. Sci. Instrum.* **2007**, *78*, 013705.
(19) Kresse, G.; Hafner, J. *Phys. Rev. B* **1993**, *47*, 558.
(20) Perdew, J. P.; Burke, K.; Ernzerhof, M. *Phys. Rev. Lett.* **1996**, *77*, 3865.
(21) Kresse, G.; Joubert, D. *Phys. Rev. B* **1999**, *59*, 1758.
(22) Tersoff, J.; Hamann, D. R. *Phys. Rev. B* **1985**, *31*, 805.
(23) Diebold, U. *Surf. Sci. Rep.* **2003**, *48*, 53.
(24) Brookes, I. M.; Muryn, C. A.; Thornton, G. *Phys. Rev. Lett.* **2001**, *87*, 266103.
(25) Schaub, R.; Thostrup, P.; Lopez, N.; Lagsgaard, E.; Stensgaard, I.; Norskov, J. K.; Besenbacher, F. *Phys. Rev. Lett.* **2001**, *87*, 266104.
(26) Wendt, S.; Matthiesen, J.; Schaub, R.; Vestergaard, E. K.; Laegsgaard, E.; Besenbacher, F.; Hammer, B. *Phys. Rev. Lett.* **2006**, *96*, 066107.
(27) Bikondoa, O.; Pang, C. L.; Ithnin, R.; Muryn, C. A.; Onishi, H.; Thornton, G. *Nat. Mat.* **2006**, *5*, 189.
(28) Henderson, M. A.; White, J. M.; Uetsuka, H.; Onishi, H. *J. Am. Chem. Soc.* **2003**, *125*, 14974.
(29) Suzuki, S.; Fukui, K.-i.; Onishi, H.; Iwasawa, Y. *Phys. Rev. Lett.* **2000**, *84*, 2156.
(30) Lane, C. D.; Petrik, N. G.; Orlando, T. M.; Kimmel, G. A. *J. Phys. Chem. C* **2007**, *111*, 16319.
(31) Szczepankiewicz, S. H.; Moss, J. A.; Hoffmann, M. R. *J. Phys. Chem. B* **2002**, *106*, 2922.
(32) Attwood, A. L.; Murphy, D. M.; Edwards, J. L.; Egerton, T. A.; Harrison, R. W. *Res. Chem. Intermed.* **2003**, *29*, 449.
(33) Coronado, J. M.; Maira, A. J.; Conesa, J. C.; Yeung, K. L.; Augugliaro, V.; Soria, J. *Langmuir* **2001**, *17*, 5368.
(34) Antcliff, K. L.; Murphy, D. M.; Griffiths, E.; Giamello, E. *Phys. Chem. Chem. Phys.* **2003**, *5*, 4306.

JP807030N